PHYSICAL REVIEW D **92,** 094518 (2015)

# Nucleon electric dipole moment with the gradient flow: The $\theta$-term contribution

Andrea Shindler,* Thomas Luu, and Jordy de Vries

*Institute for Advanced Simulation, Institut für Kernphysik, Jülich Center for Hadron Physics, JARA HPC, Forschungszentrum Jülich, D-52425 Jülich, Germany*

(Received 13 August 2015; published 30 November 2015)

We propose a new method to calculate electric dipole moments induced by the strong QCD $\theta$ term. The method is based on the gradient flow for gauge fields and is free from renormalization ambiguities. We test our method by computing the nucleon electric dipole moments in pure Yang-Mills theory at several lattice spacings, enabling a first-of-its-kind continuum extrapolation. The method is rather general and can be applied for any quantity computed in a $\theta$ vacuum. This first application of the gradient flow has been successful and demonstrates proof-of-principle, thereby providing a novel method to obtain precise results for nucleon and light nuclear electric dipole moments.

DOI: 10.1103/PhysRevD.92.094518 PACS numbers: 12.38.Gc, 11.30.Er, 12.38.-t, 14.20.Dh

## I. INTRODUCTION

The electric dipole moments (EDMs) of the neutron and proton are very sensitive probes of $CP$-violating sources beyond those contained in the Standard Model (SM). In fact, the current bound on the neutron EDM strongly constrains many models of beyond-the-SM (BSM) physics. At current experimental accuracies, a nonzero nucleon EDM cannot be accounted for by the phase in the quark-mass matrix. This implies that such a signal is either caused by a nonzero QCD $\theta$ term or by genuine BSM physics which, at low energies, can be parametrized in terms of higher-dimensional $CP$-violating quark-gluon operators. Irrespective of the origin, the signal for the nucleon EDM will be small and largely masked by strong-interaction physics, which presents a formidable challenge to the interpretation of such a signal. To disentangle the origin of a nonzero EDM measurement (e.g. $\theta$ term or BSM), a quantitative understanding of the underlying hadronic physics is required.

The current experimental limit on the neutron EDM is $|d_N| < 2.9 \cdot 10^{-13}$ $e$ fm [1] and experiments are underway to improve this bound by 1 to 2 orders of magnitude. The bound on the proton EDM is induced from the $^{199}$Hg EDM limit [2] and is $|d_P| < 7.9 \cdot 10^{-12}$ $e$ fm. Plans exist to probe the EDM of the proton directly (and other light nuclei) in storage rings [3] with a proposed sensitivity of $10^{-16}$ $e \cdot$ fm, thus improving the current bounds by several orders of magnitudes and covering a wide range where BSM physics can show its footprint.

Nucleon EDMs arising from the QCD $\theta$ term or BSM physics have been calculated both in models [4] and in chiral perturbation theory [5,6]. In the latter approach, the nucleon EDMs are calculated in terms of effective $CP$-odd hadronic interactions that have the same symmetry properties as the underlying $CP$-odd sources at the quark level (for a review, see [7]). The calculated EDMs depend on several low-energy constants (LECs) whose sizes are in most cases unknown and need to be estimated or calculated with lattice QCD.

Lattice QCD can thus be used to perform an *ab initio* calculation of the nucleon EDM. For the $\theta$ term, this has already been shown in the pioneering works in Refs. [8,9] and later in Ref. [10] (for BSM sources only the nucleon EDMs arising from the quark EDMs have been calculated with lattice QCD [11]). The chiral and infinite volume extrapolations of unpublished lattice data from Shintani *et al.* have been performed in Refs. [12,13]. The calculation of the EDM within a lattice (discretized) formulation of QCD is very nontrivial, and present large difficulties for two main reasons. The renormalization of the $CP$-odd operators and the degradation of the signal-to-noise ratio towards the chiral limit. Additionally, the $\theta$ term itself introduces an imaginary term in the real Euclidean action, which produces a sign problem and precludes the use of standard stochastic methods employed by lattice QCD. Reference [14] performed a lattice QCD calculation of the neutron EDM induced by a $\theta$ term that was analytically continued into the complex plane. This allows the usage of standard stochastic methods.

In this paper we propose, without relying on any complex rotation of the $\theta$ term, a method based on the gradient flow for the gauge fields [15] that has no renormalization ambiguities and, to our knowledge, is the only method that allows a theoretical sound continuum limit. A first account of this method can be found in Ref. [16].

The remainder of the paper is organized as follows: The next section gives a cursory discussion of the

*Corresponding author.
a.shindler@fz-juelich.de

 

phenomenology of the nucleon EDM. In Sec. III we introduce definitions and our method. Section IV discusses the gradient flow for gauge fields and its relevance to the calculations presented in this paper. We provide details of our lattice calculations and their results in Secs. V and VI, followed by a discussion in the ensuing section.

## II. PHENOMENOLOGY OF THE QCD THETA TERM

The discrete space-time symmetries parity $P$, time-reversal $T$, and the combination of charge conjugation and parity $CP$, are broken in QCD by the QCD $\theta$ term. In the case of three quark flavors the QCD action is given by

$$S_\theta = \int d^4x[\mathcal{L}_{\rm QCD} - i\theta q(x)], \tag{1}$$

where $\mathcal{L}_{\rm QCD}$ is the standard Euclidean QCD Lagrangian

$$\mathcal{L}_{\rm QCD} = \frac{1}{4g^2}F^a_{\mu\nu}F^{a,\mu\nu} + \bar\psi(\gamma_\mu D_\mu + M)\psi \tag{2}$$

and

$$q(x) = \frac{1}{64\pi^2}\epsilon_{\mu\nu\rho\sigma}F^a_{\mu\nu}(x)F^a_{\rho\sigma}(x), \tag{3}$$

is the topological charge density. The fermion field containing up, down and strange quarks is denoted by $\psi = (u,d,s)^T$ and $F^a_{\mu\nu}$ is the gluon field strength tensor. $\epsilon_{\mu\nu\alpha\beta}$ ($\epsilon_{0123} = +1$) is the completely antisymmetric tensor, $D_\mu$ the gauge-covariant derivative, $M$ the real $3\times 3$ quark-mass matrix, and $\theta$ the coupling of the $CP$-odd interaction. In Eq. (2) the complex phase of the quark-mass matrix has been absorbed in the physical parameter $\theta$, i.e. we choose a fermionic basis where the $CP$-odd interaction comes solely from the topological charge density.

The most important consequence of the QCD $\theta$ term is that it induces EDMs of hadrons and nuclei. The first dedicated EDM experiment was the neutron EDM experiment in 1957 [17]. Since then, the accuracy of the measurement has been improved by 6 orders of magnitude without finding a signal. The current bound $d_N < 2.9\cdot 10^{-13} e\cdot$ fm [1] sets strong limits on the size of $\theta$ and sources of $CP$ violation from physics beyond the SM.

In order to set a bound on the $\theta$ term, it is necessary to calculate the dependence of the neutron EDM on $\theta$. One way to do this is by using $\chi$PT. This calculation has been done up to next-to-leading order (NLO) in both $SU(2)$ [6,18,19] and $SU(3)$ [5,20,21] $\chi$PT. Focusing here on the two-flavored theory, the neutron ($d_N$) and proton EDM ($d_P$) are given by:

$$d_N = \frac{eg_A\bar g_0^\theta}{16\pi^2F_\pi^2}\left(\ln\frac{M_\pi^2}{\Lambda^2_{N,\rm EDM}} - \frac{\pi M_\pi}{2M_N}\right), \tag{4}$$

$$d_P = -\frac{eg_A\bar g_0^\theta}{16\pi^2F_\pi^2}\left(\ln\frac{M_\pi^2}{\Lambda^2_{P,\rm EDM}} - \frac{2\pi M_\pi}{M_N}\right), \tag{5}$$

in terms of $g_A \simeq 1.27$ the strong pion-nucleon coupling constant, $F_\pi \simeq 92.2$ MeV the pion decay constant, $M_\pi$ and $M_N$ the pion and nucleon mass respectively, $e>0$ the proton charge, and, in principle, three low-energy constants (LECs) of $CP$-odd chiral interactions: $\bar g_0^\theta$ and $\bar d_{N,P}$. The first one, $\bar g_0^\theta$, is not free as discussed below [see Eq. (9)]. The latter two are absorbed in renormalization-scale, $\mu$, independent constants

$$\Lambda_{N,\rm EDM} = \mu\,\exp\left\{-\frac{8\pi^2F_\pi^2\bar d_N(\mu)}{eg_A\bar g_0^\theta}\right\}, \tag{6}$$

$$\Lambda_{P,\rm EDM} = \mu\,\exp\left\{\frac{8\pi^2F_\pi^2\bar d_P(\mu)}{eg_A\bar g_0^\theta}\right\}. \tag{7}$$

The first term in brackets in Eqs. (4) and (5) arises from the leading-order one-loop diagram involving the $CP$-odd vertex

$$\mathcal{L}_{\pi N}(\theta) = -\frac{\bar g_0^\theta}{2F_\pi}\bar N\vec\pi\cdot\vec\tau N, \tag{8}$$

in terms of the nucleon doublet $N$ and the pion triplet $\vec\pi$. The LO loop is divergent and the divergence and associated scale dependence have been absorbed into the counter terms $\bar d_{N,P}$ which signify contributions to the nucleon EDMs from short-range dynamics and appear at the same order as the LO loop diagrams. The second term in brackets in Eqs. (4) and (5) is a next-to-leading-order correction.

The $\theta$ term breaks chiral symmetry as a complex quark mass. As such, chiral symmetry relates $\bar g_0^\theta$ to known $CP$-even LECs [21,22]. In particular, it is possible to write [23]

$$\begin{aligned}\frac{\bar g_0^\theta}{2F_\pi} &= \frac{(M_N - M_P)^{\rm strong}}{2F_\pi}\frac{m_\star}{\bar m\varepsilon}\theta \\ &= (15.5\pm 2.5)\times 10^{-3}\theta,\end{aligned} \tag{9}$$

where $(M_N - M_P)^{\rm strong}$ is the quark-mass induced part of the proton-neutron mass splitting, $\bar m = (m_u+m_d)/2$, $m_\star = m_u m_d/(m_u+m_d)$, and $\varepsilon = (m_u - m_d)/(m_u + m_d)$. To get a rough estimate of the sizes of the nucleon EDMs, we can insert Eq. (9) in Eqs. (5) and (4). If we assume that $\Lambda_{\rm EDM} \simeq M_N$, we obtain

$$d_N \simeq -2.1\times 10^{-3}\theta\, e\,\text{fm}, \tag{10}$$

$$d_P \simeq +2.5\times 10^{-3}\theta\, e\,\text{fm}, \tag{11}$$

as a rough estimate of the nucleon EDMs. A comparison with the experimental bound then gives the strong constraint $\theta \le 10^{-10}$. Clearly, a more reliable constraint on $\theta$

requires a first-principle calculation of the nucleon EDMs. In the isospin limit, $\bar{g}_0^\theta$ scales as $\bar{m} \sim M_\pi^2$ such that the loop contributions to the EDMs vanish in the chiral limit as $M_\pi^2 \log M_\pi^2$ (see Eqs. (4) and (5).

In the isoscalar combination $d_N + d_P$ the loop contribution cancels out to a large extent. For observables sensitive to this combination, such as the deuteron EDM [24,25], a first-principle calculation of the total nucleon EDM is important to differentiate the $\theta$ term from possible BSM sources of $CP$ violation [26,27]. In the specific case of the isoscalar combination a precise evaluation of disconnected diagrams is needed in any lattice QCD calculation.

## III. THE ELECTRIC DIPOLE MOMENT

The theory is defined in Euclidean space with the action given in Eq. (1). The EDM of a nucleon is related to the spatial charge density distribution. If we define the quark charges as $Q_u = 2/3\,e$ and $Q_d = Q_s = -1/3\,e$, the nucleon EDMs are obtained from the matrix element of the electromagnetic current

$$J_\mu(x) = Q_u \bar{u}(x)\gamma_\mu u(x) + Q_d \bar{d}(x)\gamma_\mu d(x) + Q_s \bar{s}(x)\gamma_\mu s(x), \tag{12}$$

between nucleon states in the $\theta$ vacuum,

$$\langle N^\theta(\mathbf{p}', s')|J_\mu|N^\theta(\mathbf{p}, s)\rangle = \bar{u}_N^\theta(\mathbf{p}', s')\Gamma_\mu(Q^2)u_N^\theta(\mathbf{p}, s). \tag{13}$$

$\Gamma_\mu(Q^2)$ has the most general four-vector structure consistent with the symmetries of the action (1) such as gauge, O(4), $C$ and $CPT$ invariance. Note that the photon momentum $q = p' - p$ in Euclidean space is

$$Q_\mu = (Q_4, \mathbf{Q}) = (iq^0, \mathbf{q}),$$
$$Q^2 = -(q^0)^2 + |\mathbf{q}|^2 = -q^2. \tag{14}$$

Following Ref. [8] the $Q^2$ dependence of the matrix element is parametrized by a linear combination of $CP$-even and $CP$-odd form factors. Using Euclidean O(4) rotational invariance, gauge symmetry and the spurionic symmetry $P \times \theta \to -\theta$, the most general decomposition reads

$$\Gamma_\mu(Q^2) = g(\theta^2)\Gamma_\mu^{\text{even}}(Q^2) + i\theta h(\theta^2)\Gamma_\mu^{\text{odd}}(Q^2), \tag{15}$$

where $g$, $h$ are even functions of $\theta$. The $CP$-even contribution is given by

$$\Gamma_\mu^{\text{even}}(Q^2) = \gamma_\mu F_1(Q^2) + \sigma_{\mu\nu}\frac{Q_\nu}{2M}F_2(Q^2) \tag{16}$$

where the Dirac and Pauli form factors $F_1$ and $F_2$ are related to the electric and the magnetic form factors

$$G_E(Q^2) = F_1(Q^2) - \frac{Q^2}{4M^2}F_2(Q^2),$$
$$G_M(Q^2) = F_1(Q^2) + F_2(Q^2). \tag{17}$$

The $CP$-odd term reads

$$\Gamma_\mu^{\text{odd}}(Q^2) = \sigma_{\mu\nu}\gamma_5\frac{Q_\nu}{2M}F_3(Q^2). \tag{18}$$

In the literature $\Gamma_\mu^{\text{odd}}(Q^2)$ usually contains an additional parity violating form factor, the anapole form factor. The anapole form factor breaks parity symmetry but does not break time reversal, i.e. is $CP$-even while breaking both $C$ and $P$. It, therefore, does not contribute to the amplitude in Eq. (13) of the electromagnetic current evaluated in a $\theta$ vacuum. In other words, the $\theta$ term alone cannot induce a nucleon anapole form factor. The EDM is directly related to the $CP$-odd $F_3(Q^2)$ form factor at zero momentum transfer,

$$d_N = \theta g(\theta^2)\frac{F_3^N(0)}{2M_N} \simeq \theta\frac{F_3^N(0)}{2M_N} + O(\theta^3). \tag{19}$$

In lattice calculations, matrix elements can be extracted from the large-distance behavior of appropriate correlation functions in Euclidean space-time. In the case at hand, one considers three-point correlations such as

$$G_{NJ_\mu N}^\theta = \langle \mathcal{N} J_\mu \overline{\mathcal{N}}\rangle_\theta, \tag{20}$$

where $\mathcal{N}$ is an interpolating operator with the same quantum number of the nucleon. The three-point functions are to be evaluated with the Euclidean action $S_\theta$. Although the action with $\theta \neq 0$ cannot be directly studied by numerical Monte Carlo methods, in the small $\theta$ limit one can obtain the desired result for EDM by expanding around $\theta = 0$ and taking only the linear term in $\theta$. That is, for a generic expectation value of product of operators, $\mathcal{O}$, in a $\theta$ vacuum, we can write

$$\langle \mathcal{O}\rangle_\theta \simeq \langle \mathcal{O}\rangle_{\theta=0} + i\theta\langle \mathcal{O}\int d^4x\, q(x)\rangle_{\theta=0} + \mathrm{O}(\theta^2), \tag{21}$$

where $q(x)$ is the topological charge density (3). The experimental bound on $\theta$ is currently $\theta < O(10^{-10})$ (see Sec. II), thus a power expansion in $\theta$ is well justified.[1]

In general this proposal could be hampered by the impossibility of giving a sound or practical definition on the lattice of the topological charge density and its continuum limit. In this work we propose to directly compute the matrix element

[1]Alternatively, the nucleon EDM at finite $\theta$ can be also determined using reweighting techniques with the complex weight factor $e^{i\theta Q}$.

$$\langle \mathcal{O} \int d^4x\, q(x) \rangle_{\theta=0}, \tag{22}$$

using the gradient flow (see Sec. IV) to define the topological charge density [15]. By doing so, we have a theoretically sound definition of the correlation function with no renormalization ambiguities and a well-defined continuum limit.

## IV. GRADIENT FLOW AND THE TOPOLOGICAL SUSCEPTIBILITY

The gradient flow [15] of Yang-Mills gauge fields is defined as follows

$$\partial_t B_\mu = D_{\nu,t} G_{\nu\mu}, \tag{23}$$

where the flow time $t$ has a time-squared dimension,

$$\begin{aligned} G_{\mu\nu} &= \partial_\mu B_\nu - \partial_\nu B_\mu + [B_\mu, B_\nu], \\ D_{\mu,t} &= \partial_\mu + [B_\mu, \cdot], \end{aligned} \tag{24}$$

and the initial condition on the flow-time-dependent field $B_\mu(t,x)$ at $t=0$ is given by the fundamental gauge field. The gradient flow for gauge fields and for fermions [28] has several applications and here we mention the definition of a relative scale [15,29], the determination of the strong coupling constant [15,30] and of the chiral condensate [28,31], the calculation of the energy-momentum tensor [32,33] and of the topological susceptibility [34,35]. We have recently proposed to use the gradient flow for the determination of the strange content of the nucleon [16].

One way to understand the flow equations is to consider them as steepest descent equations in the space of gauge fields. As such the evolution along the flow drives the gauge configurations towards local minima of the action. The topological charge is defined at nonvanishing flow time as

$$\mathcal{Q}(t) = \int d^4x\, q(x,t), \tag{25}$$

with

$$q(x,t) = \frac{1}{64\pi^2} \epsilon_{\mu\nu\rho\sigma} G^a_{\mu\nu}(x,t) G^a_{\rho\sigma}(x,t). \tag{26}$$

In Fig. 1 we show the flow-time evolution of $\mathcal{Q}(t)$ evaluated on two representatives of our gauge ensembles. Rather rapidly $\mathcal{Q}(t)$ reaches a plateau where it assumes an almost integer value saturating the corresponding instanton bound.

Another way to understand the effect of the gradient flow on the gauge fields is apparent already at tree-level. The smoothing at short distances over a range $\sqrt{8t}$ corresponds in momentum space to a Gaussian damping of the large momenta. This results in a very interesting property of the flowed gauge fields $B_\mu(x,t)$: they are free from ultraviolet divergences [15,36] for all $t>0$ and do not require any renormalization. This powerful result can be used to simplify the renormalization pattern of operators involving gauge fields. In general, one would need to relate the local operators evaluated at nonvanishing flow times with the ones at zero flow times. The case of the topological charge and all the correlation functions containing the topological charge is special, because in this case we can define the topological charge, and for example the topological susceptibility, directly at nonvanishing flow time [15]. The Euclidean theory is prepared on a lattice of spacing $a$ and volume $L^3 \times T$. The calculations in this and the following sections have been performed with the standard Wilson gauge action, with $\beta = 6/g^2$, at 4 different lattice spacings $a = 0.093,\ 0.079,\ 0.068,\ 0.048$ fm corresponding to $\beta = 6.0,\ 6.1,\ 6.2,\ 6.45$. In this work we use the Sommer scale [37,38], $r_0 = 0.5$ fm, to fix the lattice spacing in physical units. The size of the box is respectively $L/a = 16,\ 24,\ 24,\ 32$ with $T/L = 2$. To generate the gauge links, we have used a heat bath algorithm with a ratio of number of over-relaxation steps, $N_{\rm OR}$, over a number of Cabibbo-Marinari updates, $N_{\rm HB}$, per sweep of $N_{\rm OR}/N_{\rm HB} = 4/1$. For thermalization we have performed 2000 updates. For the finest lattice spacing, we have

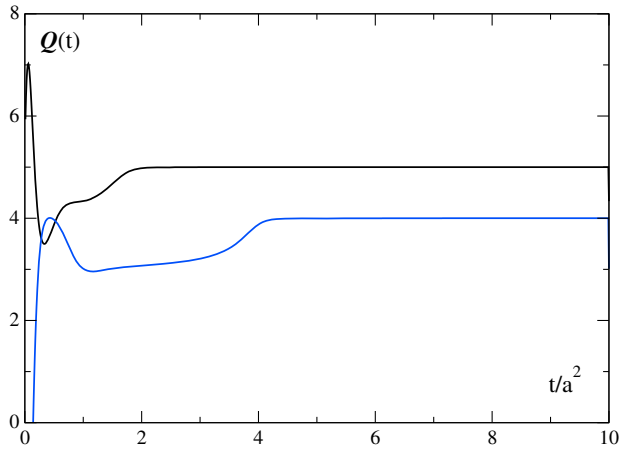


FIG. 1 (color online). Flow-time dependence of the topological charge for two different gauge fields.

TABLE I. Summary of our runs: $N_{\rm th}$ is the number of thermalization updates, $N_{\rm up}$ is the total number of updates, $N_g$ is the number of gauges saved and $N_{\rm meas}$ is the number of gauges analyzed.

| $\beta$ | $N_{\rm th}$ | $N_{\rm up}$ | $N_g$ | $N_{\rm meas}$ |
|---|---|---|---|---|
| 6.0 | 2000 | 200000 | 1000 | 1000 |
| 6.1 | 2000 | 65000 | 325 | 325 |
| 6.2 | 2000 | 60000 | 300 | 300 |
| 6.45 | 2000 | 122400 | 612 | 153 |

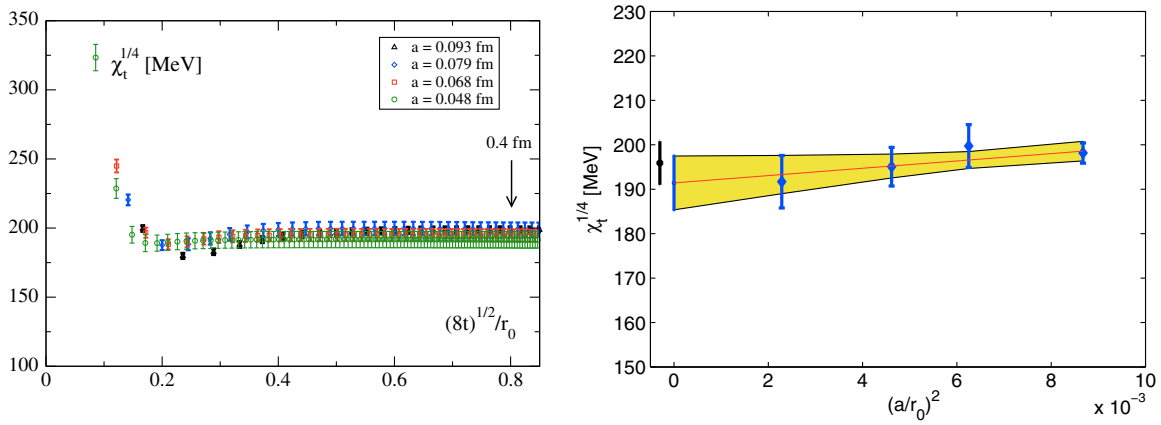


FIG. 2 (color online). Left plot: flow-time dependence of the topological susceptibility at several lattice spacings. Right plot: continuum limit of the topological susceptibility. The yellow band is a linear extrapolation in $a^2$ compared with a constant fit.

analyzed all correlation functions skipping 800 gauges while for the remaining correlation functions we have skipped 200 gauges. A summary of parameter runs is given in Table I.

With these choices we have observed no significant autocorrelation for all our lattice spacings. We obtain the same outcome also for the correlation functions used for the determination of the EDMs. A more detailed discussion of autocorrelations for the fermionic correlation functions is given in Sec. V.

The gradient flow equation at finite lattice spacing is solved following Appendix C of Ref. [15] with step size for the flow time $\epsilon = 0.01$. The topological charge density is defined as in Eq. (26) where $G^a_{\mu\nu}(x,t)$ is the lattice implementation of the field tensor defined in Ref. [39]. Any other definition of the topological charge density in a pure Yang-Mills theory requires a finite multiplicative renormalization [40] that has to be determined as a function of the bare coupling, in order to perform the continuum limit. With the definition based on the gradient flow, this renormalization factor is 1, independently of the lattice action used. Using the definition of the topological charge density at nonvanishing flow time given above, we can also define the topological susceptibility,

$$\chi_{\rm t}(t) = \frac{1}{V}\int d^4x d^4y \langle q(t,x) q(t,y)\rangle. \tag{27}$$

The topological susceptibility defined as in Eq. (27), but at vanishing flow time $t = 0$, not only needs a multiplicative renormalization, but, more importantly, has a $1/a^4$ power divergence.[2] However, with the definition at nonvanishing flow time, the topological susceptibility needs no renormalization and it has a well defined continuum limit. We have computed $\chi_t$ for several lattice spacings as a function of the flow time. In the left plot of Fig. 2 we show the topological susceptibility in physical units as a function of $\sqrt{8t}/r_0$. The divergence-free property of the gauge fields at nonvanishing flow time allows us to perform the continuum limit at fixed value of $\sqrt{8t}/r_0$. In the continuum limit we expect the topological susceptibility to be flow-time independent for every positive flow time, $\sqrt{8t}/r_0 > 0$ [15].

For small flow-time values we observe two different effects. First, for $\sqrt{8t} \lesssim 0.1$ fm we observe a rapid increase of $\chi_t$ that is just a reflection of the short distance singularities discussed above. Second, for 0.1 fm $\lesssim \sqrt{8t} \lesssim$ 0.2 fm we observe some discretization effects. For $\sqrt{8t} > 0.2$ fm we find complete agreement between all lattice spacings and, as expected, $\chi_t$ is flow-time independent. We perform the continuum limit at $\sqrt{8t}/r_0 = 0.8$ and this is shown in the right plot of Fig. 2 where we compare a linear extrapolation in $a^2$ with a constant one. We decide to quote as final result

$$[\chi_{\rm t}]^{1/4} = 195.9(4.9)\ \text{MeV}, \tag{28}$$

that is a constant fit including all lattice spacings. The values at all lattice spacings and different extrapolations to the continuum limit are listed in Table II. This result is in

TABLE II. Numerical results for the topological susceptibility and the $CP$-odd mixing angle $\alpha_N^{(1)}$ for several lattice spacings. The continuum extrapolated values are obtained with a constant fit using the 3 finest lattice spacings (fit 1) and a linear extrapolation in $a^2$ using all the lattice spacings (fit 2).

| $a^2 \times 10^3$[fm$^2$] | $\chi_t^{1/4}$[MeV] | $\alpha_N$ |
|---|---|---|
| 8.675135 | 198.1(2.3) | 0.289(19) |
| 6.250475 | 199.7(4.8) | 0.314(38) |
| 4.615747 | 195.1(4.3) | 0.324(33) |
| 2.285814 | 191.7(5.9) | 0.301(35) |
| 0 [fit 1] | 195.9(4.9) | 0.314(35) |
| 0 [fit 2] | 191.4(6.0) | 0.326(40) |

[2]A notable exception is the definition of the topological susceptibility proposed in Ref. [41] based on spectral projectors.

perfect agreement with the result [42] obtained using the index theorem with a chiral lattice Dirac operator and the result [43] obtained using the spectral projector method. Very recently a paper has been submitted with a precise determination of the topological susceptibility [44] using the gradient flow. The results are consistent within statistical uncertainties.

## V. *CP*-BROKEN VACUUM AND NUCLEON MIXING

The form factor $F_3$, directly related to the nucleon EDM, defined in Eq. (18) can be computed nonperturbatively with suitable ratios of the following two- and three-point functions in a $\theta$ vacuum

$$G^{\theta}_{NN}(\mathbf{p}, x_0) = a^3 \sum_{\mathbf{x}} e^{i\mathbf{p}\mathbf{x}} \langle \mathcal{N}(\mathbf{x}, x_0) \overline{\mathcal{N}}(0) \rangle_{\theta}, \quad (29)$$

$$G^{\theta}_{NJ_\mu N}(\mathbf{p}_1, \mathbf{p}_2, x_0, y_0) = a^6 \sum_{\mathbf{x},\mathbf{y}} e^{i\mathbf{p}_2(\mathbf{x}-\mathbf{y})} e^{i\mathbf{p}_1\mathbf{y}} \times \langle \mathcal{N}(\mathbf{x}, x_0) J_\mu(\mathbf{y}, y_0) \overline{\mathcal{N}}(0) \rangle_{\theta}. \quad (30)$$

Here, the baryon interpolating fields are

$$\mathcal{N}(x) = \varepsilon_{ABC} u_A(x) [u_B^T(x) \mathcal{C}\gamma_5 d_C(x)], \quad (31)$$

$$\overline{\mathcal{N}}(x) = \varepsilon_{ABC} [\bar{u}_A^T(x) \mathcal{C}\gamma_5 \bar{d}_B^T(x)] \bar{u}_C(x), \quad (32)$$

and $\mathcal{C}$ is the charge conjugation matrix. We now describe in some detail the spectral decomposition for the two-point functions and defer to Appendix for the slightly more cumbersome spectral decomposition of the three-point functions. Most of the discussion on the spectral decomposition follows Shintani *et al.* [8], but we rederive some of their results for clarity and to be consistent with our normalizations. The key ingredient of the spectral decompositions is the matrix element of the interpolating operator of the nucleon between the $\theta$ vacuum and a single nucleon state

$$\langle \theta | \mathcal{N} | N^{\theta}(\mathbf{p}, s) \rangle = \mathcal{Z}_N(\theta) u_N^{\theta}(\mathbf{p}, s). \quad (33)$$

In a theory that does not preserve parity, for instance due to the presence of a $\theta$ term, the nucleon state does not have a definite parity and the nucleon spinor can be written as

$$u_N^{\theta}(\mathbf{p}, s) = e^{i\alpha_N(\theta)\gamma_5} u_N(\mathbf{p}, s), \quad (34)$$

where $u_N(\mathbf{p}, s)$ is the nucleon spinor in the $\theta = 0$ vacuum. In other words, the nucleon spinor satisfies the modified Dirac equation

$$(i\gamma_\mu p_\mu + M_N(\theta) e^{-i2\alpha_N(\theta)\gamma_5}) u_N^{\theta}(\mathbf{p}, s) = 0. \quad (35)$$

The theory still preserves the spurionic symmetry $P_\theta$: $P \times \theta \to -\theta$, where $P$ is the standard parity transformation. This implies that both the energies and the amplitudes $M(\theta)$, $\mathcal{Z}(\theta)$ are even functions of $\theta$, $M(\theta) = M + O(\theta^2)$ and $\mathcal{Z}_N(\theta) = \mathcal{Z}_N + O(\theta^2)$.

The phase $\alpha_N(\theta)$ plays a very important role in the determination of the EDM. From the spurionic symmetry $P_\theta$ we deduce that $\alpha_N(\theta) = -\alpha_N(-\theta)$ and for small values of $\theta$, $\alpha_N(\theta) = \alpha_N^{(1)}\theta + O(\theta^3)$. It is important to determine precisely the mixing parameter $\alpha_N$ before extracting the *CP*-odd form factors from the three-point functions. The reason is that the mixing between different parity states can induce a spurious *CP*-odd contribution to the correlation function proportional to the *CP*-even form factors. These spurious contributions can be subtracted only with a precise determination of the mixing angle $\alpha_N(\theta)$. The details of these spurious contributions and relative subtractions are detailed in the Appendix.

For on-shell nucleons with energy $-ip_0 = E_N(\mathbf{p})$ where $E_N(\mathbf{p}) = \sqrt{|\mathbf{p}|^2 + M_N^2}$, the infinite volume normalization reads

$$\langle N^{\theta}(\mathbf{q}, s) | N^{\theta}(\mathbf{k}, s') \rangle = (2\pi)^3 \sqrt{2E_N(\theta; \mathbf{q})} \sqrt{2E_N(\theta; \mathbf{k})} \delta^{(3)}(\mathbf{k} - \mathbf{q}) \delta_{s,s'}. \quad (36)$$

Taking into account the parity mixing, the completeness relation of the nucleon spinors with spatial momentum $\mathbf{p}$ reads

$$\sum_s u_N^{\theta}(\mathbf{p}, s) \bar{u}_N^{\theta}(\mathbf{p}, s) = E_N(\theta; \mathbf{p})\gamma_0 - i\gamma_k p_k + M_N(\theta) e^{2i\alpha_N(\theta)\gamma_5}. \quad (37)$$

For small values of $\theta$, we have

$$\sum_s u_N^{\theta}(\mathbf{p}, s) \bar{u}_N^{\theta}(\mathbf{p}, s) = E_N(\mathbf{p})\gamma_0 - i\gamma_k p_k + M_N(1 + 2i\theta\alpha_N^{(1)}\theta\gamma_5) + O(\theta^2). \quad (38)$$

We can now perform the spectral decomposition of the nucleon two-point functions in a $\theta$ vacuum. Retaining only the one-state leading contribution we obtain

$$G^{\theta}_{NN}(\mathbf{p}, x_0) = \frac{e^{-E_N(\theta;\mathbf{p})x_0}}{2E_N(\theta; \mathbf{p})} |\mathcal{Z}_N(\theta; \mathbf{p})|^2 \sum_s u_N^{\theta}(\mathbf{p}, s) \bar{u}_N^{\theta}(\mathbf{p}, s), \quad (39)$$

and using the completeness relation we get

$$G^{\theta}_{NN}(\mathbf{p},x_0)_{\alpha\beta} = \frac{e^{-E_N(\theta;\mathbf{p})x_0}}{2E_N(\theta;\mathbf{p})}|\mathcal{Z}_N(\theta;\mathbf{p})|^2 \times [E_N(\theta;\mathbf{p})\gamma_0 - i\gamma_k p_k + M_N(\theta)e^{2i\alpha_N(\theta)\gamma_5}]_{\alpha\beta}, \quad (40)$$

where $\alpha$ and $\beta$ are the Dirac indices. Expanding the lhs of Eq. (40) in powers of $\theta$, we obtain

$$G^{\theta}_{NN}(\mathbf{p},x_0) = G_{NN}(\mathbf{p},x_0) + i\theta G^{\mathcal{Q}}_{NN}(\mathbf{p},x_0) + \mathrm{O}(\theta^2) \quad (41)$$

where

$$G_{NN}(\mathbf{p},x_0) = a^3\sum_{\mathbf{x}} e^{i\mathbf{p}\mathbf{x}}\langle \mathcal{N}(\mathbf{x},x_0)\overline{\mathcal{N}}(0)\rangle, \quad (42)$$

and

$$G^{\mathcal{Q}}_{NN}(\mathbf{p},x_0) = a^3\sum_{\mathbf{x}} e^{i\mathbf{p}\mathbf{x}}\langle \mathcal{N}(\mathbf{x},x_0)\overline{\mathcal{N}}(0)\mathcal{Q}\rangle. \quad (43)$$

The term linear in $\theta$ can be computed inserting the topological charge in the nucleon two-point function. The topological charge $\mathcal{Q}$, defined in Eq. (25), is computed as detailed in Sec. IV using the gradient flow. In this way the topological charge is free from any renormalization ambiguity and the continuum limit can be safely performed keeping fixed the flow time in physical units. To minimize discretization effects we choose, $\sqrt{8t}/r_0 = 0.8$. We omit the flow-time dependence of $\mathcal{Q}(t)$ because in this range of flow times any correlator involving the topological charge is flow time independent (see Sec. IV).

By expanding the spectral decomposition, i.e. the rhs of Eq. (40), in powers of $\theta$, we obtain the standard nucleon spectral decomposition

$$G_{NN}(\mathbf{p},x_0) = \frac{e^{-E_N(\mathbf{p})x_0}}{2E_N(\mathbf{p})}|\mathcal{Z}_N(\mathbf{p})|^2[E_N(\mathbf{p})\gamma_0 - i\gamma_k p_k + M], \quad (44)$$

and the term linear in $\theta$

$$G^{\mathcal{Q}}_{NN}(\mathbf{p},x_0) = \frac{e^{-E_N(\mathbf{p})x_0}}{2E_N(\mathbf{p})}|\mathcal{Z}_N(\mathbf{p})|^2 2M_N\alpha_N^{(1)}\gamma_5. \quad (45)$$

For simplicity we have not written down the opposite parity states propagating from $T$. If we project to $\mathbf{p} = \mathbf{0}$ and to positive parity we obtain

$$C(x_0) = \mathrm{tr}[P_+ G_{NN}(\mathbf{0},x_0)] = 2|Z_N|^2 e^{-M_N x_0} + \cdots, \quad (46)$$

and

$$C^{\mathcal{Q}}(x_0) = \mathrm{tr}[P_+\gamma_5 G^{\mathcal{Q}}_{NN}(\mathbf{0},x_0)] = 2|Z_N|^2\alpha_N^{(1)}e^{-M_N x_0} + \cdots. \quad (47)$$

We observe that the two correlators have the same leading exponential behavior. If the sampling of all topological sectors is correctly performed, the effective masses of the two correlators should agree asymptotically for large Euclidean times.

In Fig. 3 we plot the distribution of the topological charge for 4 different lattice spacings at $\sqrt{8t} = 0.8r_0$. Details on the definition can be found in Sec. IV. The distribution looks reasonably Gaussian with all average values statistically consistent with zero. We observe for $a = 0.079$ fm, that the distribution has slightly larger width, but this is related to the slightly larger physical volume of that lattice. As we have seen in the previous section, the topological susceptibility does not show any sign of discretization errors.

For the computation of the two-point functions, we have studied 3 different levels $s_i$, $i = 1, 2, 3$ of Gaussian smearing [45]. The relevant parameters of the Gaussian smearing that we have considered, usually labeled as $\{\alpha, N_G\}$, are $s_1 = \{2, 30\}$, $s_2 = \{4, 25\}$, $s_3 = \{5.5, 70\}$. We have found that the $s_3$ smearing has a better projection on the fundamental state, but it is also the smearing that adds more noise to the correlator. Compromising between an earlier plateau and a less noisier correlator, we have decided to choose the smearing $s_2$ for the 2 coarsest lattice spacings and the smearing $s_3$ for the 2 finest spacings.

The fermion lattice action is the nonperturbatively improved Wilson action [46–48]. The propagators are computed with sources located stochastically in the three spatial directions. We choose 20 stochastic spatial points for the finest lattice spacing and 10 stochastic points for the others. The rationale behind this choice is to have $\mathrm{O}(L/a)$ different stochastic points to improve the overlap between the topological charge and the fermionic part of the correlation functions. We stress that this is very important to improve the signal-to-noise ratio not only of the two-point functions, but especially for the three-point functions which we discuss in the next section.

We have performed the calculation at 4 lattice spacings (see Sec. IV) and at the following set of momenta

$$\{\mathbb{P}\} = \frac{2\pi}{L}\cdot\{(0,0,0),(\pm1,0,0),(\pm1,\pm1,0),(\pm1,\pm1,\pm1),(\pm2,0,0)\}. \quad (48)$$

The values of the quark mass for all the lattice spacings corresponds to a value of the pseudoscalar mass, $M_{\mathrm{PS}} \simeq 800$ MeV, fixed in physical units [49]. From coarser to finer spacings they correspond to the following values of the hopping parameter, $\kappa = \{0.13353, 0.13423, 0.13460, 0.13485\}$. For these values of $\kappa$ we have computed the

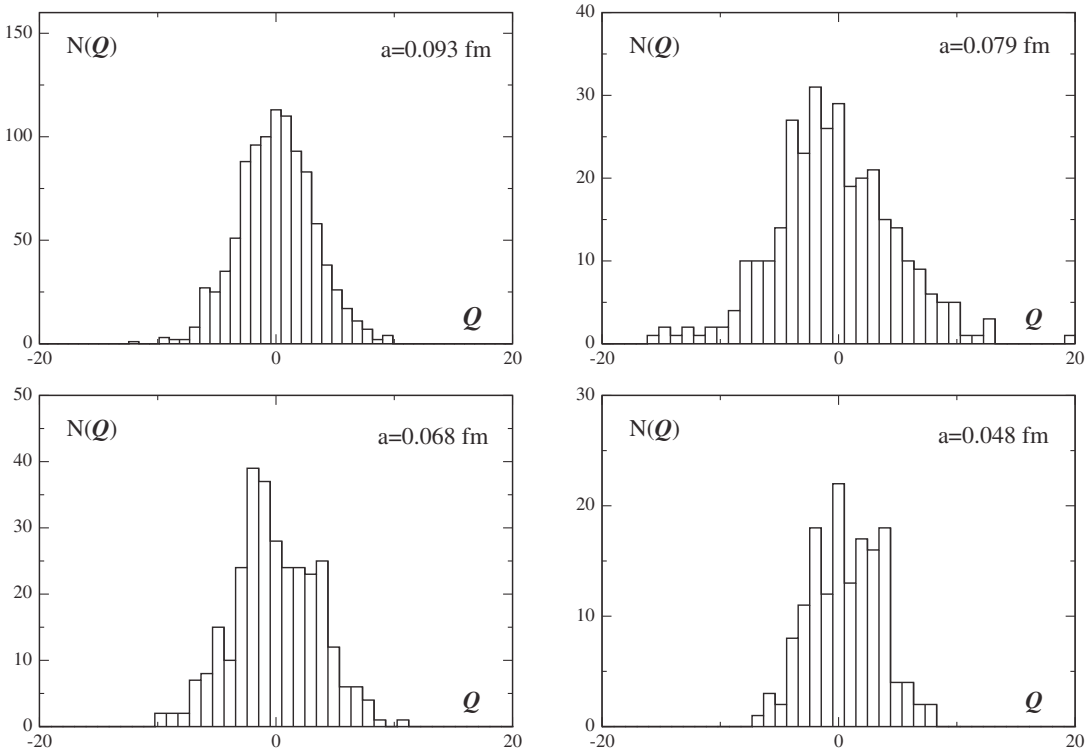


FIG. 3. Distribution of the topological charge computed for $\sqrt{8t}/r_0 = 0.8$ for 4 different lattice spacings.

nucleon mass, that shows very small discretization errors and it corresponds to a value $M_N \simeq 1.65$ GeV. We have also checked the dispersion relation for all lattice spacings and find that the discretization errors are below our statistical accuracy. In Fig. 4 we show our results for our coarsest lattice spacing of the nucleon energy squared for all the $|\mathbf{p}|^2$ of the set (48) with the continuum form of the dispersion relation.

In the left plot of Fig. 5 we show the effective masses of the two correlators in Eqs. (46), (47) for the finest lattice spacing. It is clear that for large Euclidean times we have perfect agreement between the two effective masses and

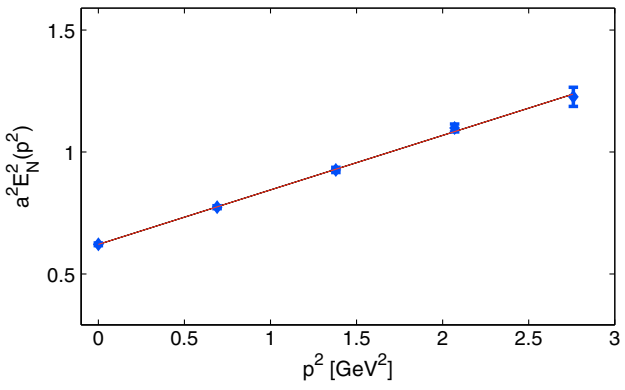


FIG. 4 (color online). Results for the nucleon energy squared at different values of $|\mathbf{p}|^2$ compared with the continuum dispersion relation $E_N^2 = M_N^2 + |\mathbf{p}|^2$.

very similar results are obtained for all the other lattice spacings we have. This is also confirmed on the right plot of Fig. 5 where we show, again for our finest spacing, the nucleon mass obtained from the 2 correlators in Eqs. (46), (47) for different fit ranges. The calculation of the mixing angle $\alpha_N^{(1)}$ is now straightforward

$$\frac{\mathrm{tr}[P_+\gamma_5 G_{NN}^{Q}(\mathbf{0}, x_0)]}{\mathrm{tr}[P_+ G_{NN}(\mathbf{0}, x_0)]} = \alpha_N^{(1)} + \cdots, \tag{49}$$

and we expect a plateau for large Euclidean times with higher-order corrections that are exponentially suppressed. In the left plot of Fig. 6 we show the Euclidean time dependence of $\alpha_N^{(1)}$ obtained from the ratio in Eq. (49) at $a = 0.048$ fm. A plateau is easily identified as is the case for all the other lattice spacings. This is just a reflection of the previous result, namely that asymptotically both correlators in Eqs. (46), (47) are dominated by the same exponential behavior with the same mass.

We have performed several checks on the calculation of the mixing angle because a solid determination of $\alpha_N^{(1)}$ is crucial for a correct and precise extraction of the nucleon EDM as detailed in the next section and in the Appendix. We can determine the mixing angle from ratios as in Eq. (49) but with correlators projected at nonvanishing spatial momenta. If we choose the same interpolating operators for the two correlators, from the spectral decomposition in Eqs. (42), (43) we obtain

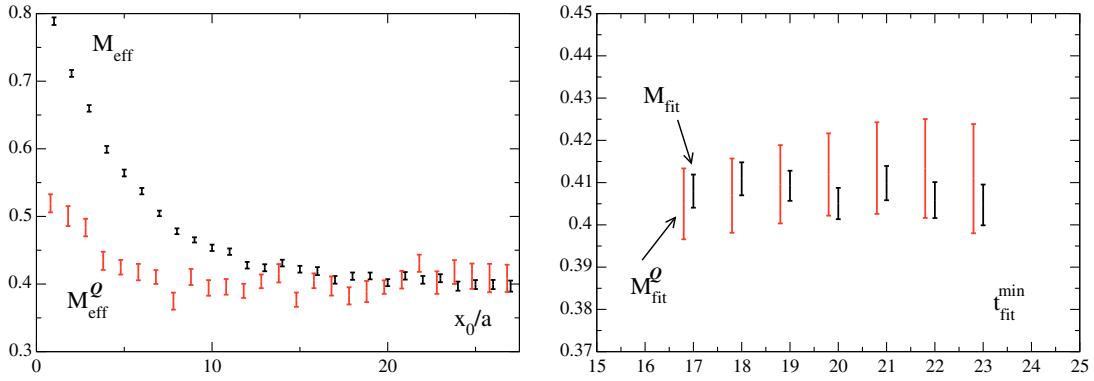


FIG. 5 (color online). Left plot: comparison of the effective masses in lattice units obtained from the nucleon correlators at $a = 0.048$ fm with and without the insertion of the topological charge, i.e. from Eq. (46) ($M_{\rm eff}$) and from Eq. (47) ($M^{\mathcal{Q}}_{\rm eff}$). Right plot: comparison of the nucleon masses in lattice units obtained with the nucleon correlators (46), $M_{\rm fit}$, and (47), $M^{\mathcal{Q}}_{\rm fit}$, at $a = 0.048$ fm for different fit ranges ($t^{\rm min}_{\rm fit}, t^{\rm max}_{\rm fit} = 28$).

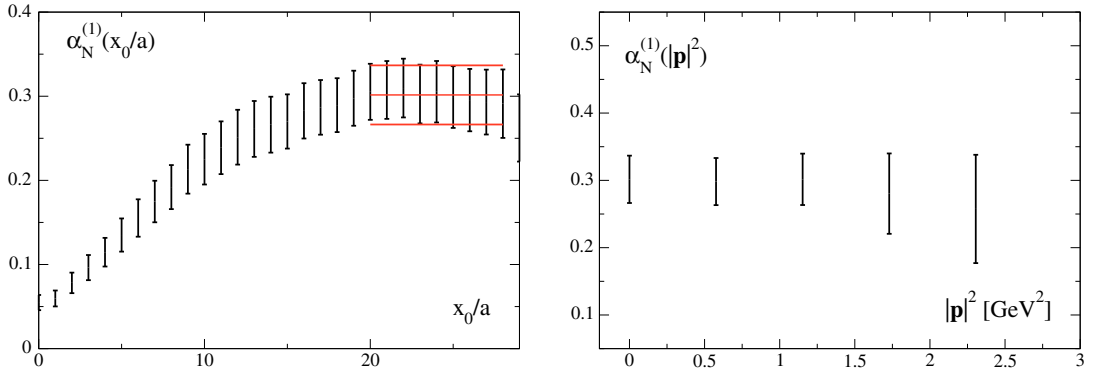


FIG. 6 (color online). Left plot: Euclidean time dependence of $\alpha_N^{(1)}$ determined from the ratio in Eq. (49) at $a = 0.048$ fm. The red band indicates our choice for the plateau and the corresponding uncertainty. Right plot: momentum dependence of $\alpha_N^{(1)}$, as determined from the ratio in Eq. (50), at $a = 0.048$ fm.

$$\frac{E_N(\mathbf{p}) + M_N}{2M_N} \frac{\mathrm{tr}[P_+ \gamma_5 G^{\mathcal{Q}}_{NN}(\mathbf{p}, x_0)]}{\mathrm{tr}[P_+ G_{NN}(\mathbf{p}, x_0)]} = \alpha_N^{(1)} + \cdots . \quad (50)$$

Up to discretization effects, $\alpha_N^{(1)}$ should not depend on the momentum chosen in the nucleon two-point functions. In the right plot of Fig. 6 we show the $|\mathbf{p}|^2$ dependence of $\alpha_N^{(1)}$ for our finest lattice spacing. We expect an increased uncertainty as we increase the nucleon momentum and we see perfect agreement between all the values of the mixing angle. We obtain similar results for all the other lattice spacings.

Another check of our calculation concerns the autocorrelation time of the correlators containing the topological charge. Critical slowing down has been observed for topological charge and susceptibility both in QCD and Yang-Mills theory [50] using an Hybrid Montecarlo (HMC) algorithm. In particular, it is expected that the problem can become relevant for lattice spacings below 0.05 fm. Even though the situation here is different because the correlators contain explicitly fermionic propagators and we do not use an HMC algorithm, at our finest lattice spacing $a = 0.048$ fm we have computed the autocorrelation function for all the Euclidean times $x_0$ of the correlator $G^{\mathcal{Q}}_{NN}(\mathbf{0}, x_0)$ and $\alpha_N^{(1)}$. We have followed Refs. [51,52] for the determination of the autocorrelation function and integrated autocorrelation times.

In the left plot of Fig. 7 we show for $\alpha_N^{(1)}$ at $x_0/a = 10$ the normalized autocorrelation function and the estimate of the integrated autocorrelation time $\tau_{\rm int}$ with an automatic windowing procedure [51]. On the right plot we show the estimate of $\tau_{\rm int}$ of $\alpha_N^{(1)}$ for all Euclidean times. It is clear there is almost no autocorrelation, $\tau_{\rm int} = 0.5$, for all Euclidean times. As a further check, we compared the error estimate of $\alpha_N^{(1)}$ using the autocorrelation function method to a standard bootstrap method. This is shown in Fig. 8 from which it becomes clear that we can safely use a boostrap analysis to determine our statistical uncertainty for all correlators at all our lattice spacings. We can now

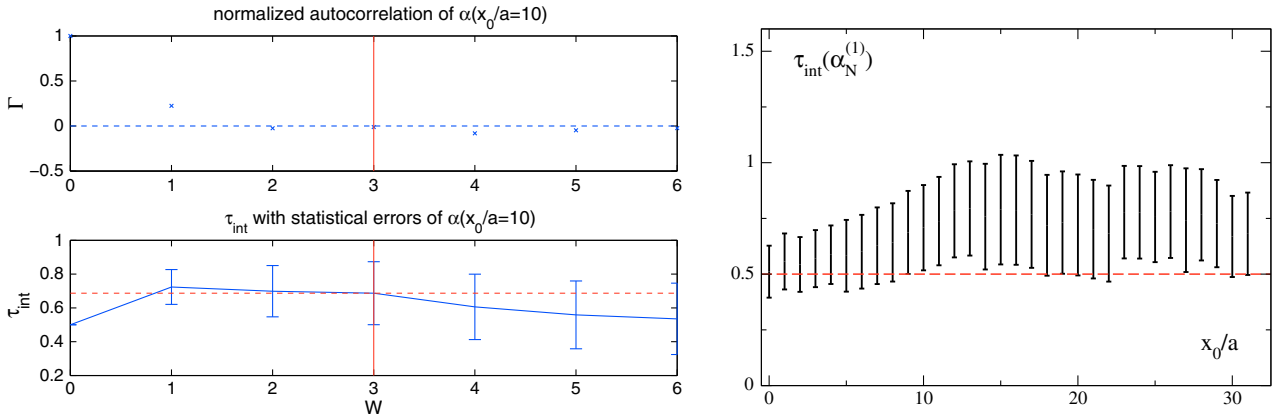


FIG. 7 (color online). Left plot: normalized autocorrelation function and estimate of the integrated autocorrelation time $\tau_{\rm int}$ with the automatic windowing procedure [51] of $\alpha_N^{(1)}$ at $x_0/a = 10$. Right plot: estimate of $\tau_{\rm int}$ of $\alpha_N^{(1)}$ for all Euclidean times. The dashed red line indicate the absence of autocorrelation, $\tau_{\rm int} = 0.5$.

perform the continuum limit of $\alpha_N^{(1)}$ for fixed value of the pion mass. In Fig. 9 we show the continuum limit and in Table II we list all the values at all lattice spacings and different extrapolations to the continuum limit. We compare a linear extrapolation in $a^2$ (yellow band) with a constant extrapolation including the three finest lattice spacings. We observe a perfect agreement for all the extrapolations and tiny discretization errors. The theory is nonperturbatively improved so we expect an $O(a^2)$ scaling behavior.

Since we see no signs of discretization errors, as a final result we quote the value obtained using a constant fit excluding the coarsest lattice spacing,

$$\alpha_N^{(1)} = 0.314(35). \tag{51}$$

We stress that this is the first time that a continuum limit is performed for this $CP$-mixing angle. The normalization chosen for $\alpha_N^{(1)}$ and the convention for the Dirac $\gamma$ matrices is consistent with the one of Ref. [9]. Our result in the continuum limit differs by $2\sigma$ from the result of Ref. [9] that is obtained with a different fermionic and gauge action, at a single lattice spacing of $a \simeq 0.15$ fm and at a similar quark mass value.

## VI. NUCLEON ELECTRIC DIPOLE MOMENT

The spectral decomposition of the three-point functions

$$G^{\theta}_{NJ_\mu N}(\mathbf{p}_1, \mathbf{p}_2, x_0, y_0) = a^6 \sum_{\mathbf{x},\mathbf{y}} e^{i\mathbf{p}_2(\mathbf{x}-\mathbf{y})} e^{i\mathbf{p}_1\mathbf{y}} \langle \mathcal{N}(\mathbf{x}, x_0) J_\mu(\mathbf{y}, y_0) \overline{\mathcal{N}}(0) \rangle_\theta, \tag{52}$$

relevant for the determination of the nucleon EDM is detailed in the Appendix and the final result for the leading exponentials is given in Eq. (A4). By taking suitable ratios

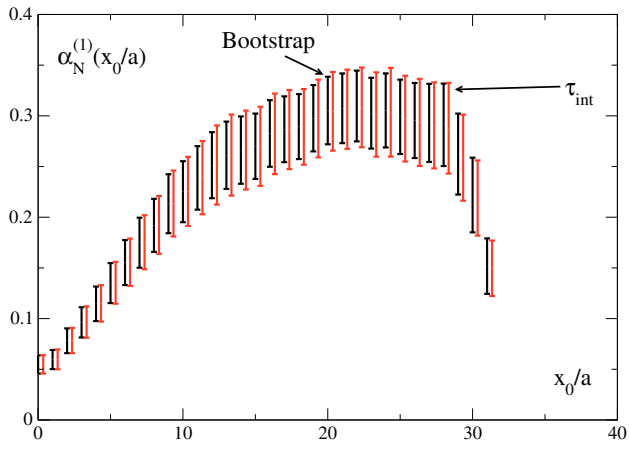


FIG. 8 (color online). Comparison of error estimates using the autocorrelation function method, labeled by $\tau_{\rm int}$, and a standard bootstrap method.

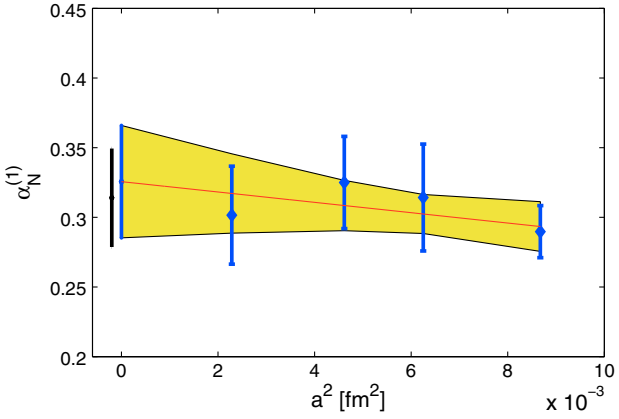


FIG. 9 (color online). Continuum limit of $\alpha_N^{(1)}$. The yellow band is a linear extrapolation in $a^2$ and it is compared with a constant extrapolation including all the lattice spacings and excluding the coarsest one.

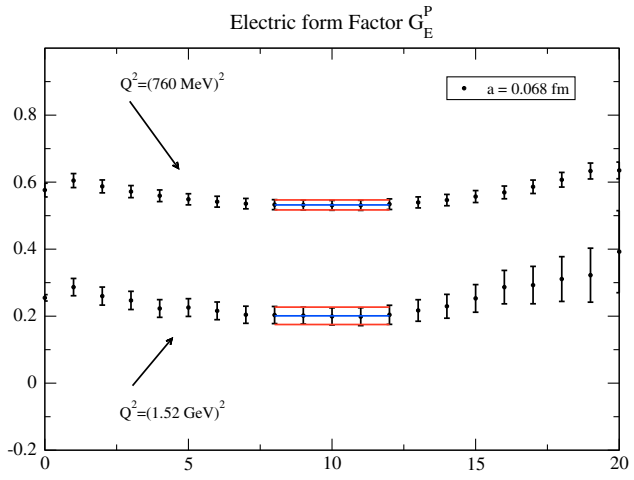


FIG. 10 (color online). Euclidean time dependence of the proton electric form factor determined from the ratio (A21) for two different values of $Q^2$.

of two- and three-point functions we can extract $CP$-even and $CP$-odd form factors defined in Eqs. (16) and (18).

The three-point functions have been computed for the set of momenta $\{\mathbb{P}\}$ defined in Eq. (48) and, when possible, we have averaged over all equivalent momenta configurations. We have tested several sink locations $x_0$ and, after some numerical experiments, we have chosen the following set,

$$\{x_0\} = (16a, 20a, 20a, 28a), \tag{53}$$

from the coarsest to the finest lattice spacing. We work in the SU(3) flavor-symmetric limit such that the disconnected contributions vanish.

For all the form factors calculations we use a local vector current. The normalization constant $Z_V(g_0^2)$ is taken from Ref. [53]. To compute the EDM we use the ratio of Eq. (A27). In order to determine $F_3(Q^2)$, we need to subtract contributions proportional to the mixing angle $\alpha_N^{(1)}$ and the $CP$-even form factors $G_E(Q^2)$ and $G_M(Q^2)$. To determine $G_E(Q^2)$ and $G_M(Q^2)$ we use the ratios in Eqs. (A21) and (A26). In Fig. 10 we show two typical plateaus for the electric form factor of the proton for 2 different momenta. A plateau is easily identified as for all the other momenta and lattice spacings. We collect in a single plot, Fig. 11, the electric form factor $G_E(Q^2)$ of the proton and the neutron including all the lattice spacings. Discretization errors are well under control. The red curve for the proton electric form factor is a fit to the lowest four momenta using the standard dipole form,

$$G_E^{\mathrm{dip}}(Q^2) = \frac{1}{\left(1+\frac{Q^2}{M_D^2}\right)^2}. \tag{54}$$

The neutron electric form factor vanishes at $Q^2 = 0$ and is rather small for larger values of $Q^2$, but we are still able to identify a clear signal over a wide range of $Q^2$. This will be important for the determination of the neutron EDM. In Fig. 12 we show the same result for the magnetic form factors and the same type of dipole fit

$$G_E^{\mathrm{dip}}(Q^2) = \frac{\kappa_{P,N}}{\left(1+\frac{Q^2}{M_D^2}\right)^2}, \tag{55}$$

where the anomalous magnetic moments $\kappa_{P,N}$ are fixed to their phenomenological values. The fit parameters $M_D^2$ are not expected to reproduce the phenomenological values (see for example Ref. [54]). We perform these fits as a check that our lattice data can be fitted by a dipole form, however we do not use these fits in the determination of the EDMs below.

With the precise determination of the $CP$-even form factors and the mixing angle $\alpha_N^{(1)}$, we can now determine the nucleon EDM. By evaluating the ratio on the lhs of

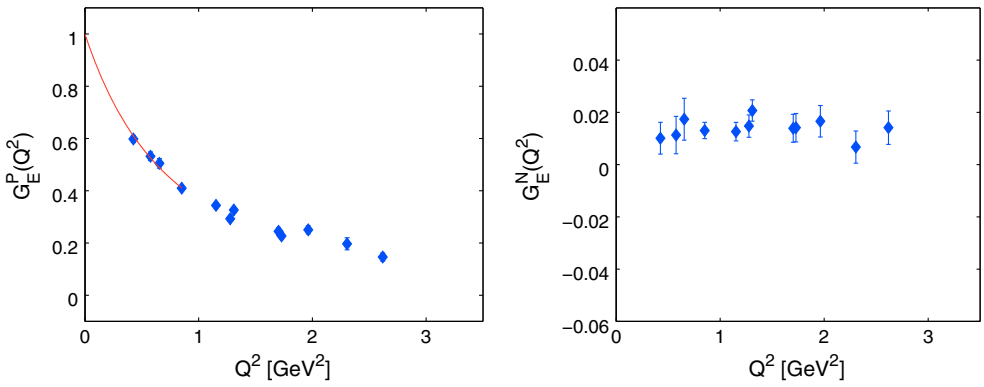


FIG. 11 (color online). Momentum dependence of the electric form factor for the proton (left plot) and the neutron (right plot). The red curve for the proton form factor is a phenomenological fit restricted to the four lowest momenta. The fit result is $M_D^2 = 1.5182(71)$ GeV$^2$ (see text).

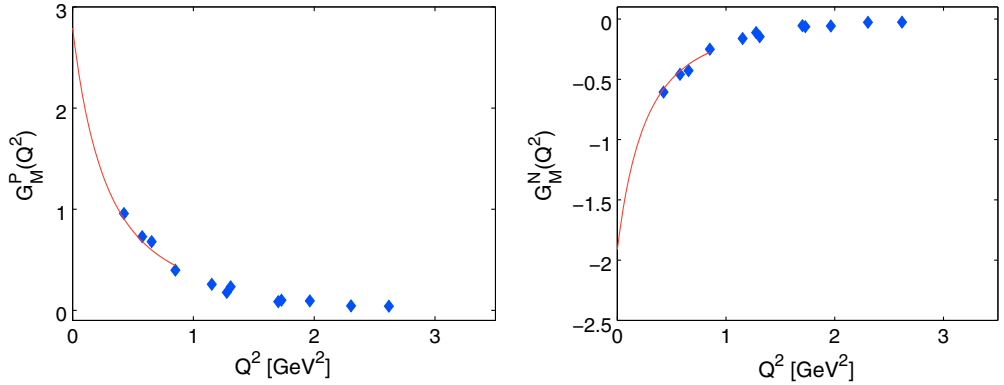


FIG. 12 (color online). Same as Fig. 11 but for the magnetic form factors. The fit results are $M_D^2 = 0.5621(20)$ GeV$^2$ for the proton and $M_D^2 = 0.5224(15)$ GeV$^2$ for the neutron.

Eq. (A27) and subtracting the spurious contributions from the r.h.s, we can determine the $CP$-odd form factor $F_3(Q^2)$. In Fig. 13 we show the plateau for the normalized $CP$-odd form factor $F_3(Q^2)/2M_N$ for all the momenta at our finest lattice spacing. For the lowest two momenta it is possible to extract a signal while for the largest two, the signal is too small and consistent with zero. In Fig. 14 we show the $Q^2$ dependence of $F_3(Q^2)/2M_N$ on a single plot including all our lattice spacings. The different lattice spacings results agree rather well, indicating small discretization errors within our statistical accuracy. For this reason, we determine the EDM by extrapolating using the three finest lattice spacings result to $Q^2 = 0$ with the same fit function. An extrapolation using all four lattice spacings give completely consistent results as shown in Fig. 14. For the extrapolation to $Q^2 = 0$, we use the SU(2) $\chi$PT result of [6] as a guideline. There the form factor is expanded as

$$\frac{F_3^{P/N}(Q^2)}{2M_N} = d_{P/N} + S_{P/N}Q^2 + H_{P/N}(Q^2). \quad (56)$$

The values at $Q^2 = 0$ are the nucleons EDMs and the slope in $Q^2$ at small $Q^2$, $S_{P/N}$, are the so called Schiff moments [55]. The functions $H_{P/N}(Q^2)$, defined in [6], scale as $Q^4$ for small $Q^2$ and they can be neglected for small enough values of $Q^2$. The numerical data for small $Q^2$ indeed suggest a linear $Q^2$ dependence. A linear extrapolation in $Q^2$, using the three finest lattice spacings, gives us the values of the proton and neutron EDMs

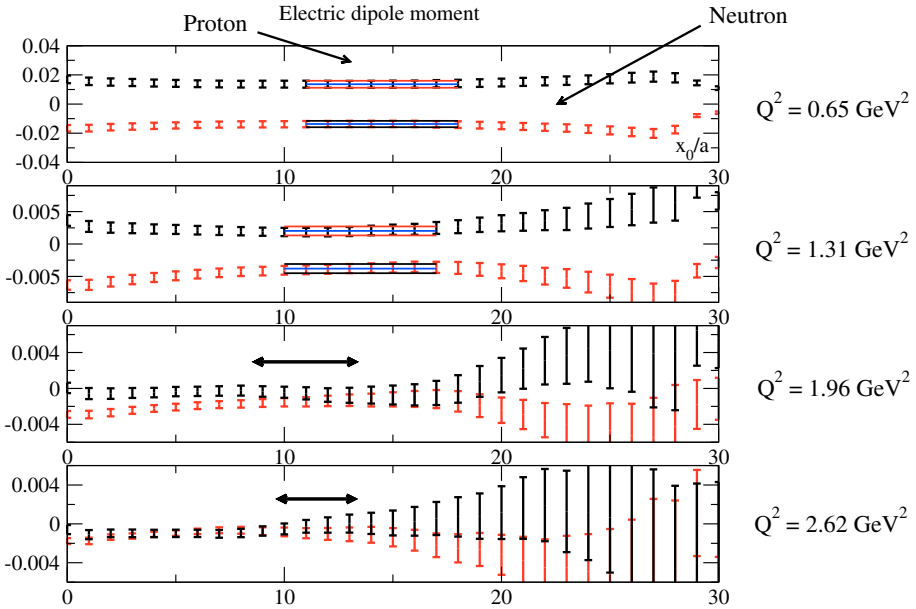


FIG. 13 (color online). Euclidean time dependence of $F_3(Q^2)/2M_N$ in $e \cdot$ fm extracted from the ratio in Eq. (A27) for the four nonvanishing lattice momenta at our finest lattice spacing.

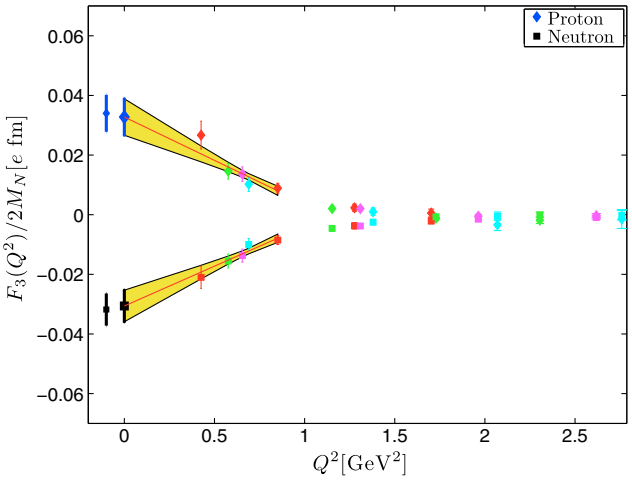


FIG. 14 (color online). Momentum dependence of the $CP$-odd form factor $F_3(Q^2)/2M_N$ of the proton and the neutron. The yellow band is a linear extrapolation in $Q^2$ as suggested from $\chi$PT at NLO using all four lattice spacings. Different colors represent different lattice spacings: $\beta = 6.0$ (cyan), $\beta = 6.1$ (red), $\beta = 6.2$ (magenta), $\beta = 6.45$ (green). As a comparison we plot, slightly displaced, the $Q^2 = 0$ extrapolation using the three finest lattice spacings.

$$d_{\mathrm{P}} = 0.0340(62)\theta\, e \cdot \mathrm{fm}, \tag{57}$$

$$d_{\mathrm{N}} = -0.0318(54)\theta\, e \cdot \mathrm{fm}. \tag{58}$$

If we make the reasonable assumption that at this relatively large value of the pseudoscalar mass, quenched and unquenched calculations give comparable results, we can try to estimate the values of the EDM at the physical point. To do so, we use as constraint the fact that the EDM in the continuum has to vanish in the chiral limit. In principle, we would like to use the $\chi$PT expressions in Eqs. (4) and (5), but considering the large pseudoscalar mass used in our calculations, the $\chi$PT expressions are not reliable and we instead perform a simple linear fit in $M_\pi^2$. We then obtain the following estimates,

$$d_{\mathrm{P}}^{\mathrm{phys}} = 0.96(18) \times 10^{-3}\theta\, e \cdot \mathrm{fm}, \tag{59}$$

$$d_{\mathrm{N}}^{\mathrm{phys}} = -0.90(15) \times 10^{-3}\theta\, e \cdot \mathrm{fm}, \tag{60}$$

where we have only included the errors from Eqs. (57) and (58). These estimates are statistically consistent with the results of [12,13]. We stress that many systematic uncertainties are not taken into account in our calculation and that the main goal of this work is to describe the new methodology and perform a first continuum extrapolation. With all the caveats intrinsic in our calculation, we can extract an upper bound for $\theta$. The experimental upper bound of the neutron EDM, $|d_N| < 2.9 \times 10^{-13}\, e\cdot$ fm, gives $\theta \lesssim 3.2 \times 10^{-10}$.

Our lattice data also allow us to extract the nucleon Schiff moments for which we obtain

$$S_{\mathrm{P}} = -1.16(33) \times 10^{-3}\theta\, e \cdot \mathrm{fm}^3, \tag{61}$$

$$S_{\mathrm{N}} = 1.07(28) \times 10^{-3}\theta\, e \cdot \mathrm{fm}^3. \tag{62}$$

In both $SU(2)$ [6,18] and $SU(3)$ [5,23] $\chi$PT, the nucleon Schiff moments are of isovector nature, in agreement with our lattice results. In fact, at leading order in the $SU(2)$ chiral expansion, the Schiff moments are predicted,

$$\begin{aligned} S_{\mathrm{P}} &= -S_{\mathrm{N}} \\ &= -\frac{e g_A \bar{g}_0^\theta}{48\pi^2 F_\pi^2 M_\pi^2} \\ &= -(1.8 \pm 0.2) \times 10^{-4}\theta\, e \cdot \mathrm{fm}^3, \end{aligned} \tag{63}$$

where we used the value of $\bar{g}_0^\theta$ given in Eq. (9).

We see that our lattice results are roughly 5 times larger than the leading-order $\chi$PT predictions which are in principle pion-mass independent (note that $\bar{g}_0^\theta \sim M_\pi^2$). However, already at the physical pion mass, the nucleon Schiff moments obtain $\mathcal{O}(60\%)$ next-to-leading-order corrections that scale as $\sim M_\pi$ [5,6]. Considering the large pseudoscalar mass used in our calculation, the discrepancy is not very worrisome.

To conclude, we have shown that it is possible to obtain a nonperturbative determination of the Schiff moments from the $Q^2$ dependence of the $CP$-odd form factor, $F_3$. With more precise lattice data at smaller pion masses, the extraction of the nucleon Schiff moments can be used for a direct determination of the LEC $\bar{g}_0$. In this way, from the pion mass dependence of the EDMs [see Eqs. (5), (4)], it is then possible to extract the other LECs, $\Lambda_{P,N}$ (or equivalently $\bar{d}_{N,P}$), from lattice QCD alone without relying on Eq. (9).

## VII. FINAL REMARKS

We have presented a first-of-its-kind continuum limit for the $CP$-mixing angle $\alpha_N$ and the nucleon EDMs. At the same time, we have performed a first *ab initio* calculation of the nucleon Schiff moments in the continuum limit which can be used to extract the value of the $CP$-odd pion-nucleon coupling constant $\bar{g}_0$. The key ingredient is the use of the gradient flow for the definition of the topological charge which, in this way, is free of renormalization ambiguities and allows a straightforward continuum extrapolation. The method we have proposed is general and can be used for any quantity computed in a $\theta$ vacuum such as EDMs of light nuclei. To test this new method we have performed the calculation in the Yang-Mills theory at a relatively large value of the quark mass. We are currently extending this calculation to QCD with dynamical configurations and smaller quark masses.

Previous calculations of nucleon EDMs [8,9] also applied a perturbative expansion in $\theta$, but instead used a cooling procedure to define the topological charge. We do believe that such calculations give the right qualitative answer, but we stress that defining the EDM in this way does not allow for a controlled continuum limit. Another method that has been proposed is to consider an imaginary $\theta$ term in the action [14]. With an imaginary $\theta$ the action becomes real and amenable to numerical Monte Carlo methods, but it requires the generation of a new gauge ensemble for each value of $\theta$. The range of $\theta$ used for the generation of these ensembles is $\theta \simeq 0.5$–$2.5$. If the calculation is performed with a Wilson-type action, the $\theta$ coefficient needs to be renormalized in order to restore the proper anomalous Ward identity. Additionally, the analytic continuation back to a real value of $\theta$ has to be done with care in regions outside the perturbative regime in $\theta$. These complications are avoided completely with our proposal, because we directly compute the linear coefficient of $\theta$ in the standard QCD background.

As a last remark we recall that with a Wilson-type fermion action, EDMs are not guaranteed to vanish in the chiral limit, which only happens after the continuum limit has been performed. The same phenomenon takes place for the topological susceptibility [35]. It is only *after* performing the continuum limit that it is possible to constrain the $\theta$-induced EDM to vanish in the chiral limit. This stresses the importance of performing the continuum limit prior to any chiral limit and we believe that our method is optimal in this respect.

We consider this work as a first step in the determination of $\theta$ and beyond-the-Standard-Model matrix elements with the gradient flow. Other contributions to EDMs, for instance from fermionic operators such as quark chromoelectric dipole moments, can be determined using the gradient flow for fermions [28], and work in this direction is in progress.

## ACKNOWLEDGMENTS

We thank R. Edwards and B. Joó for help with CHROMA [56]. We thank U.-G. Meißner for a careful reading of the manuscript. This work (J. d. V.) is supported in part by the DFG and the NSFC through funds provided to the Sino-German CRC 110 "Symmetries and the Emergence of Structure in QCD" (Grant No. 11261130311). The authors gratefully acknowledge the computing time granted by the JARA-HPC Vergabegremium and provided on the JARA-HPC Partition part of the supercomputer JUQUEEN at Forschungszentrum Jülich.

## APPENDIX: SPECTRAL DECOMPOSITION OF THE THREE-POINT FUNCTIONS

In this appendix we discuss in some detail the spectral decomposition of the three-point functions used to determine the nucleon form factors in a $\theta$ vacuum. For completeness we remind that in our calculations the initial momentum is $p_1 = ((p_1)_0, \mathbf{p}_1)$ and the final momentum is $p_2 = ((p_2)_0, \mathbf{p}_2)$. The momentum transfer is $q = p_2 - p_1 = (E(\mathbf{p}_2) - E(\mathbf{p}_1), \mathbf{p}_2 - \mathbf{p}_1)$.

If we retain only the leading exponential contribution, the spectral decomposition of the three-point functions,

$$G^{\theta}_{NJ_\mu N}(\mathbf{p}_1, \mathbf{p}_2, x_0, y_0) = a^6 \sum_{\mathbf{x},\mathbf{y}} e^{i\mathbf{p}_1\mathbf{y}} e^{i\mathbf{p}_2(\mathbf{x}-\mathbf{y})} \langle \mathcal{N}(\mathbf{x}, x_0) J_\mu(\mathbf{y}, y_0) \overline{\mathcal{N}}(0) \rangle_\theta, \quad \text{(A1)}$$

is given by

$$\begin{aligned} G^{\theta}_{NJ_\mu N}(\mathbf{p}_1, \mathbf{p}_2; x_0, y_0) = {} & \frac{e^{-E_N(\mathbf{p}_1) y_0}}{2E_N(\mathbf{p}_1)} \frac{e^{-E_N(\mathbf{p}_2)(x_0 - y_0)}}{2E_N(\mathbf{p}_2)} \\ & \times \sum_{s,s'} \langle \theta | \mathcal{N} | N^\theta(\mathbf{p}_2, s') \rangle \\ & \times \langle N^\theta(\mathbf{p}_2, s') | J_\mu | N^\theta(\mathbf{p}_1, s) \rangle \\ & \times \langle N^\theta(\mathbf{p}_1, s) | \overline{\mathcal{N}} | \theta \rangle. \end{aligned} \quad \text{(A2)}$$

Following the parametrization in Eq. (15) and using the completeness relation, we obtain for small values of $\theta$

$$\begin{aligned} & G^{\theta}_{NJ_\mu N}(\mathbf{p}_1, \mathbf{p}_2; x_0, y_0)_{\alpha\beta} \\ & = \frac{e^{-E_N(\mathbf{p}_1) y_0}}{2E_N(\mathbf{p}_1)} \frac{e^{-E_N(\mathbf{p}_2)(x_0 - y_0)}}{2E_N(\mathbf{p}_2)} \mathcal{Z}^*_N(\mathbf{p}_1) \mathcal{Z}_N(\mathbf{p}_2) \\ & \quad \times \{ [E_N(\mathbf{p}_2)\gamma_0 - i\gamma_k (p_2)_k + M_N(1 + 2i\theta\alpha^{(1)}_N \theta\gamma_5)] \Gamma_\mu(Q^2) \\ & \quad \times [E_N(\mathbf{p}_1)\gamma_0 - i\gamma_k (p_1)_k + M_N(1 + 2i\theta\alpha^{(1)}_N \theta\gamma_5)] \}_{\alpha\beta}, \end{aligned} \quad \text{(A3)}$$

where $\alpha\beta$ are the Dirac indices. If we expand in powers of $\theta$ the rhs of Eq. (A1), we obtain

$$\begin{aligned} G^{\theta}_{NJ_\mu N}(\mathbf{p}_1, \mathbf{p}_2, x_0, y_0) = {} & G_{NJ_\mu N}(\mathbf{p}_1, \mathbf{p}_2, x_0, y_0) \\ & + i\theta G^{\mathcal{Q}}_{NJ_\mu N}(\mathbf{p}_1, \mathbf{p}_2, x_0, y_0), \end{aligned} \quad \text{(A4)}$$

where

$$\begin{aligned} G_{NJ_\mu N}(\mathbf{p}_1, \mathbf{p}_2, x_0, y_0) = {} & a^6 \sum_{\mathbf{x},\mathbf{y}} e^{i\mathbf{p}_1\mathbf{y}} e^{i\mathbf{p}_2(\mathbf{x}-\mathbf{y})} \\ & \times \langle \mathcal{N}(\mathbf{x}, x_0) J_\mu(\mathbf{y}, y_0) \overline{\mathcal{N}}(0) \rangle \end{aligned} \quad \text{(A5)}$$

is the three-point function in the standard QCD background, and

$$G^{\mathcal{Q}}_{NJ_\mu N}(\mathbf{p}_1, \mathbf{p}_2, x_0, y_0) = a^6 \sum_{\mathbf{x},\mathbf{y}} e^{i\mathbf{p}_1\mathbf{y}} e^{i\mathbf{p}_2(\mathbf{x}-\mathbf{y})} \langle \mathcal{N}(\mathbf{x}, x_0) J_\mu(\mathbf{y}, y_0) \overline{\mathcal{N}}(0) \mathcal{Q} \rangle \quad \text{(A6)}$$

contains the insertion of the topological charge evaluated at nonvanishing flow time $\sqrt{8t} = 0.8 r_0$.

Depending on the form factor we are interested in, we can select the appropriate Dirac indices with appropriate projectors that we indicate generically as $\Pi$, obtaining

$$G_\mu^\theta(\mathbf{p}_1,\mathbf{p}_2;x_0,y_0;\Pi)=\mathrm{Tr}[\Pi G^\theta_{NJ_\mu N}(\mathbf{p}_1,\mathbf{p}_2;x_0,y_0)], \tag{A7}$$

i.e.

$$\begin{aligned}G_\mu^\theta(\mathbf{p}_1,\mathbf{p}_2;x_0,y_0;\Pi)=&\frac{e^{-E_N(\mathbf{p}_1)y_0}}{2E_N(\mathbf{p}_1)}\frac{e^{-E_N(\mathbf{p}_2)(x_0-y_0)}}{2E_N(\mathbf{p}_2)}\mathcal{Z}_N^*(\mathbf{p}_1)\mathcal{Z}_N(\mathbf{p}_2)\\&\times\mathrm{Tr}\{\Pi[E_N(\mathbf{p}_2)\gamma_0-i\gamma_k(p_2)_k+M_N(1+2i\theta\alpha_N^{(1)}\gamma_5)]\Gamma_\mu(Q^2)\\&\times[E_N(\mathbf{p}_1)\gamma_0-i\gamma_k(p_1)_k+M_N(1+2i\theta\alpha_N^{(1)}\gamma_5)]\}.\end{aligned} \tag{A8}$$

The spectral decomposition of the correlation functions in Eqs. (A5) and (A6) traced with a generic projector $\Pi$ are easily obtained,

$$\begin{aligned}G_\mu(\mathbf{p}_1,\mathbf{p}_2;x_0,y_0;\Pi)=&\frac{e^{-E_N(\mathbf{p}_1)y_0}}{2E_N(\mathbf{p}_1)}\frac{e^{-E_N(\mathbf{p}_2)(x_0-y_0)}}{2E_N(\mathbf{p}_2)}\mathcal{Z}_N^*(\mathbf{p}_1)\mathcal{Z}_N(\mathbf{p}_2)\mathrm{Tr}\{\Pi[E_N(\mathbf{p}_2)\gamma_0-i\gamma_k(p_2)_k+M_N]\\&\times\Gamma_\mu^{\mathrm{even}}(Q^2)[E_N(\mathbf{p}_1)\gamma_0-i\gamma_k(p_1)_k+M_N]\},\end{aligned} \tag{A9}$$

$$\begin{aligned}G_\mu^{\mathcal{Q}}(\mathbf{p}_1,\mathbf{p}_2;x_0,y_0;\Pi)=&\frac{e^{-E_N(\mathbf{p}_1)y_0}}{2E_N(\mathbf{p}_1)}\frac{e^{-E_N(\mathbf{p}_2)(x_0-y_0)}}{2E_N(\mathbf{p}_2)}\mathcal{Z}_N^*(\mathbf{p}_1)\mathcal{Z}_N(\mathbf{p}_2)\{\mathrm{Tr}[\Pi(2M_N\alpha_N^{(1)}\gamma_5)\Gamma_\mu^{\mathrm{even}}(Q^2)(E_N(\mathbf{p}_1)\gamma_0-i\gamma_k(p_1)_k+M_N)]\\&+\mathrm{Tr}[\Pi(E_N(\mathbf{p}_2)\gamma_0-i\gamma_k(p_2)_k+M_N)\Gamma_\mu^{\mathrm{even}}(Q^2)(2M_N\alpha_N^{(1)}\gamma_5)]\\&+\mathrm{Tr}[\Pi(E_N(\mathbf{p}_2)\gamma_0-i\gamma_k(p_2)_k+M_N)\Gamma_\mu^{\mathrm{odd}}(Q^2)(E_N(\mathbf{p}_1)\gamma_0-i\gamma_k(p_1)_k+M_N)]\},\end{aligned} \tag{A10}$$

where $\Gamma_\mu^{\mathrm{even}}$ and $\Gamma_\mu^{\mathrm{odd}}$ are defined in Eqs. (16) and (18). From this expression we already see that the three-point function with the insertion of the topological charge is not directly proportional to the $CP$-odd form factor $F_3$ but it contains additional contributions proportional to $\alpha_N^{(1)}$ and the $CP$-even form factors.

To extract the form factors traditionally, one defines the following chain of ratios,

$$\begin{aligned}&R_\mu^\theta(\mathbf{p}_1,\mathbf{p}_2;x_0,y_0;\Pi)\\&\quad=\frac{G_\mu^\theta(\mathbf{p}_1,\mathbf{p}_2;x_0,y_0;\Pi)}{C(\mathbf{p}_2,x_0)}\cdot K(\mathbf{p}_1,\mathbf{p}_2;x_0,y_0),\end{aligned} \tag{A11}$$

where $C(\mathbf{p},x_0)$, the nucleon two-point function, is defined as

$$\begin{aligned}C(\mathbf{p},x_0)&=\mathrm{tr}[P_+G_{NN}(\mathbf{p},x_0)]\\&=|Z_N(\mathbf{p})|^2\frac{e^{-E_N(\mathbf{p})x_0}}{E_N(\mathbf{p})}(E_N(\mathbf{p})+M_N)+\cdots\end{aligned} \tag{A12}$$

and

$$K(\mathbf{p}_1,\mathbf{p}_2;x_0,y_0)=\left[\frac{C(\mathbf{p}_2,x_0)C(\mathbf{p}_2,y_0)C(\mathbf{p}_1,x_0-y_0)}{C(\mathbf{p}_1,x_0)C(\mathbf{p}_1,y_0)C(\mathbf{p}_2,x_0-y_0)}\right]^{1/2}. \tag{A13}$$

For small $\theta$ we have

$$\begin{aligned}&R_\mu^\theta(\mathbf{p}_1,\mathbf{p}_2;x_0,y_0;\Pi)\\&\quad=R_\mu(\mathbf{p}_1,\mathbf{p}_2;x_0,y_0;\Pi)+i\theta R_\mu^{\mathcal{Q}}(\mathbf{p}_1,\mathbf{p}_2;x_0,y_0;\Pi),\end{aligned} \tag{A14}$$

where

$$\begin{aligned}&R_\mu(\mathbf{p}_1,\mathbf{p}_2;x_0,y_0;\Pi)\\&\quad=\frac{G_\mu(\mathbf{p}_1,\mathbf{p}_2;x_0,y_0;\Pi)}{C(\mathbf{p}_2,x_0)}\cdot K(\mathbf{p}_1,\mathbf{p}_2;x_0,y_0),\end{aligned} \tag{A15}$$

and

$$\begin{aligned}&R_\mu^{\mathcal{Q}}(\mathbf{p}_1,\mathbf{p}_2;x_0,y_0;\Pi)\\&\quad=\frac{G_\mu^{\mathcal{Q}}(\mathbf{p}_1,\mathbf{p}_2;x_0,y_0;\Pi)}{C(\mathbf{p}_2,x_0)}\cdot K(\mathbf{p}_1,\mathbf{p}_2;x_0,y_0).\end{aligned} \tag{A16}$$

Performing the spectral decomposition and retaining only the fundamental state, we obtain

$$R_\mu^\theta(\mathbf{p}_1,\mathbf{p}_2;x_0,y_0;\Pi) = \mathcal{N}(\mathbf{p}_1,\mathbf{p}_2)\mathrm{Tr}\{\Pi[E_N(\mathbf{p}_2)\gamma_0 - i\gamma_k(p_2)_k + M_N(1+2i\theta\alpha_N^{(1)}\theta\gamma_5)]\Gamma_\mu(Q^2) \times [E_N(\mathbf{p}_1)\gamma_0 - i\gamma_k(p_1)_k + M_N(1+2i\theta\alpha_N^{(1)}\theta\gamma_5)]\}, \tag{A17}$$

where the normalization is given by

$$\mathcal{N}(\mathbf{p}_1,\mathbf{p}_2) = \frac{1}{4E_N(\mathbf{p}_1)E_N(\mathbf{p}_2)} \times \left[\frac{E_N(\mathbf{p}_1)E_N(\mathbf{p}_2)}{(E_N(\mathbf{p}_1)+M)(E_N(\mathbf{p}_2)+M)}\right]^{1/2}. \tag{A18}$$

The ratio (A11) is defined to remove the leading exponential contributions and have a plateau for $0 \ll y_0 \ll x_0$ proportional to the form factors.

We can now specialize the projector $\Pi$, the external kinematics, and the current component in order to compute the form factors we want. For the 2 $CP$-even form factors we choose

(i) $\Pi = P_+$, $\mu = 0$, $\mathbf{p}_1 = \mathbf{p}$, $\mathbf{p}_2 = 0$.
In this case we indicate $E(\mathbf{p}) = E$ and $E(\mathbf{p}_2) = M$

$$R_0(\mathbf{p},\mathbf{0};x_0,y_0;P_+) = \mathcal{N}(\mathbf{p},\mathbf{0})\cdot 4M_N(E_N(\mathbf{p})+M_N) \times \left[F_1(Q^2) - \frac{Q^2}{4M_N^2}F_2(Q^2)\right], \tag{A19}$$

where

$$\mathcal{N}(\mathbf{p},\mathbf{0}) = \frac{1}{4M_N}\left[\frac{1}{2E_N(\mathbf{p})(E_N(\mathbf{p})+M_N)}\right]^{1/2}. \tag{A20}$$

Putting everything together, we obtain

$$R_0(\mathbf{p},\mathbf{0};x_0,y_0;P_+) = \left[\frac{E_N(\mathbf{p})+M_N}{2E_N(\mathbf{p})}\right]^{1/2} \times \left[F_1(Q^2) - \frac{Q^2}{4M_N^2}F_2(Q^2)\right]. \tag{A21}$$

To obtain Eq. (A21) and some of the equations below, we have used the following kinematic relations,

$$|\mathbf{q}|^2 = |\mathbf{p}|^2 = E_N^2 - M_N^2, \tag{A22}$$

and

$$\begin{aligned} q^2 &= (M_N - E_N)^2 - |\mathbf{q}|^2 \Rightarrow q^2 \\ &= (M_N - E_N)^2 - (E_N^2 - M_N^2) \Rightarrow q^2 \\ &= 2M_N(M_N - E_N) < 0. \end{aligned} \tag{A23}$$

This implies that

$$E_N - M_N = -\frac{q^2}{2M_N} = \frac{Q^2}{2M_N}. \tag{A24}$$

Any of the relations in Eq. (A23) define the $Q^2 = -q^2$ to be used when analyzing the form factors:

(ii) $\Pi = iP_+\gamma_5\gamma_j$, $\mu = i$, $\mathbf{p}_1 = \mathbf{p}$, $\mathbf{p}_2 = 0$.
After some algebra we obtain

$$R_i(\mathbf{p},\mathbf{0};x_0,y_0;iP_+\gamma_5\gamma_j) = \mathcal{N}(\mathbf{p},\mathbf{0})\cdot 4Mq_k\epsilon_{ijk}[F_1(Q^2)+F_2(Q^2)], \tag{A25}$$

and using the expression for the normalization (A20), we obtain

$$R_i(\mathbf{p},\mathbf{0};x_0,y_0;iP_+\gamma_5\gamma_j) = \left[\frac{1}{2E_N(\mathbf{p})(E_N(\mathbf{p})+M_N)}\right]^{1/2} \times q_k\epsilon_{ijk}[F_1(Q^2)+F_2(Q^2)]. \tag{A26}$$

For the $CP$-odd form factor there are several choices for the Dirac projector. The analysis presented in this paper uses

(i) $\Pi = iP_+\gamma_5\gamma_i$, $\mu = 0$, $\mathbf{p}_1 = \mathbf{p}$, $\mathbf{p}_2 = 0$.
If we compute the coefficient of $i\theta$, we obtain after some algebra

$$\begin{aligned} R_0^{\mathcal{Q}}(\mathbf{p},\mathbf{0};x_0,y_0;iP_+\gamma_5\gamma_i) &= \mathcal{N}(\mathbf{p},\mathbf{0}) \\ &\times \left\{-4\alpha_N^{(1)}M_Nq_i\left[F_1(Q^2) + \frac{E_N+3M_N}{2M_N}F_2(Q^2)\right] \right. \\ &\left. - 2(E_N+M_N)q_iF_3(Q^2)\right\}. \end{aligned} \tag{A27}$$

Here the importance of a precise determination of $\alpha_N^{(1)}$ becomes clear. The mixing of parity states induces spurious contributions to the correlation functions proportional to the $CP$-even form factors. These contributions need to be subtracted in order to determine the nucleon EDM.

[1] C. Baker *et al.*, Phys. Rev. Lett. **97**, 131801 (2006).
[2] W. C. Griffith, M. D. Swallows, T. H. Loftus, M. V. Romalis, B. R. Heckel, and E. N. Fortson, Phys. Rev. Lett. **102**, 101601 (2009).
[3] J. Pretz (JEDI Collaboration), Hyperfine Interact. **214**, 111 (2013).
[4] M. Pospelov and A. Ritz, Ann. Phys. (Berlin) **318**, 119 (2005).
[5] K. Ottnad, B. Kubis, U.-G. Meißner, and F.-K. Guo, Phys. Lett. B **687**, 42 (2010).
[6] E. Mereghetti, J. de Vries, W. Hockings, C. Maekawa, and U. van Kolck, Phys. Lett. B **696**, 97 (2011).
[7] E. Mereghetti and U. van Kolck, Annu. Rev. Nucl. Part. Sci. **65**, 215 (2015).
[8] E. Shintani, S. Aoki, N. Ishizuka, K. Kanaya, Y. Kikukawa, Y. Kuramashi, M. Okawa, Y. Taniguchi, A. Ukawa, and T. Yoshié, Phys. Rev. D **72**, 014504 (2005).
[9] F. Berruto, T. Blum, K. Orginos, and A. Soni, Phys. Rev. D **73**, 054509 (2006).
[10] E. Shintani, S. Aoki, and Y. Kuramashi, Phys. Rev. D **78**, 014503 (2008).
[11] T. Bhattacharya, V. Cirigliano, R. Gupta, H.-W. Lin, and B. Yoon, arXiv:1506.04196 [Phys. Rev. Lett. (to be published)].
[12] F.-K. Guo and U.-G. Meißner, J. High Energy Phys. 12 (2012) 097.
[13] T. Akan, F.-K. Guo, and U.-G. Meißner, Phys. Lett. B **736**, 163 (2014).
[14] F.-K. Guo, R. Horsley, U.-G. Meißner, Y. Nakamura, H. Perlt, P. E. L. Rakow, G. Schierholz, A. Schiller, and J. M. Zanotti, Phys. Rev. Lett. **115**, 062001 (2015).
[15] M. Lüscher, J. High Energy Phys. 08 (2010) 071.
[16] A. Shindler, J. de Vries, and T. Luu, *Proc. Sci.*, LATTICE (2014) 251.
[17] E. Purcell and N. Ramsey, Phys. Rev. **78**, 807 (1950).
[18] W. Hockings and U. van Kolck, Phys. Lett. B **605**, 273 (2005).
[19] D. O'Connell and M. J. Savage, Phys. Lett. B **633**, 319 (2006).
[20] B. Borasoy, Phys. Rev. D **61**, 114017 (2000).
[21] R. Crewther, P. Di Vecchia, G. Veneziano, and E. Witten, Phys. Lett. **88B**, 123 (1979).
[22] E. Mereghetti, W. Hockings, and U. van Kolck, Ann. Phys. (Amsterdam) **325**, 2363 (2010).
[23] J. de Vries, E. Mereghetti, and A. Walker-Loud, Phys. Rev. C **92**, 045201 (2015).
[24] J. de Vries, R. Higa, C.-P. Liu, E. Mereghetti, I. Stetcu, R. G. E. Timmermans, and U. van Kolck, Phys. Rev. C **84**, 065501 (2011).
[25] J. Bsaisou, C. Hanhart, S. Liebig, U.-G. Meißner, A. Nogga, and A. Wirzba, Eur. Phys. J. A **49**, 31 (2013).
[26] O. Lebedev, K. A. Olive, M. Pospelov, and A. Ritz, Phys. Rev. D **70**, 016003 (2004).
[27] W. Dekens, J. de Vries, J. Bsaisou, W. Bernreuther, C. Hanhart, Ulf-G. Meißner, A. Nogga, and A. Wirzba, J. High Energy Phys. 07 (2014) 069.
[28] M. Lüscher, J. High Energy Phys. 04 (2013) 123.
[29] S. Borsanyi *et al.*, J. High Energy Phys. 09 (2012) 010.
[30] P. Fritzsch and A. Ramos, J. High Energy Phys. 10 (2013) 008.
[31] A. Shindler, Nucl. Phys. **B881**, 71 (2014).
[32] H. Suzuki, Prog. Theor. Exp. Phys. **2013**, 83B03 (2013).
[33] L. Del Debbio, A. Patella, and A. Rago, J. High Energy Phys. 11 (2013) 212.
[34] A. Chowdhury, A. Harindranath, J. Maiti, and P. Majumdar, J. High Energy Phys. 02 (2014) 045.
[35] M. Bruno, S. Schaefer, and R. Sommer (ALPHA Collaboration), J. High Energy Phys. 08 (2014) 150.
[36] M. Lüscher and P. Weisz, J. High Energy Phys. 02 (2011) 051.
[37] R. Sommer, Nucl. Phys. **B411**, 839 (1994).
[38] S. Necco and R. Sommer, Nucl. Phys. **B622**, 328 (2002).
[39] S. O. Bilson-Thompson, D. B. Leinweber, and A. G. Williams, Ann. Phys. (Amsterdam) **304**, 1 (2003).
[40] E. Vicari and H. Panagopoulos, Phys. Rep. **470**, 93 (2009).
[41] L. Giusti and M. Luscher, J. High Energy Phys. 03 (2009) 013.
[42] L. Del Debbio, L. Giusti, and C. Pica, Phys. Rev. Lett. **94**, 032003 (2005).
[43] M. Luscher and F. Palombi, J. High Energy Phys. 09 (2010) 110.
[44] M. Cé, C. Consonni, G. P. Engel, and L. Giusti, Phys. Rev. D **92**, 074502 (2015).
[45] S. Gusken, Nucl. Phys. B, Proc. Suppl. **17**, 361 (1990).
[46] B. Sheikholeslami and R. Wohlert, Nucl. Phys. **B259**, 572 (1985).
[47] M. Lüscher, S. Sint, R. Sommer, and P. Weisz, Nucl. Phys. **B478**, 365 (1996).
[48] M. Luscher, S. Sint, R. Sommer, P. Weisz, and U. Wolff, Nucl. Phys. **B491**, 323 (1997).
[49] J. Garden, J. Heitger, R. Sommer, and H. Wittig (ALPHA and UKQCD Collaboration), Nucl. Phys. **B571**, 237 (2000).
[50] S. Schaefer, R. Sommer, and F. Virotta (ALPHA Collaboration), Nucl. Phys. **B845**, 93 (2011).
[51] U. Wolff (ALPHA Collaboration), Comput. Phys. Commun. **156**, 143 (2004).
[52] N. Madras and A. D. Sokal, J. Stat. Phys. **50**, 109 (1988).
[53] M. Luscher, S. Sint, R. Sommer, and H. Wittig, Nucl. Phys. **B491**, 344 (1997).
[54] M. Belushkin, H.-W. Hammer, and U.-G. Meißner, Phys. Rev. C **75**, 035202 (2007).
[55] S. D. Thomas, Phys. Rev. D **51**, 3955 (1995).
[56] R. G. Edwards and B. Joo (SciDAC, LHPC, and UKQCD Collaboration), Nucl. Phys. B, Proc. Suppl. **140**, 832 (2005).